From Blue to White to Yellow Emitter: A Hexanuclear Copper Iodide Nanocluster

Ke Xu[a], Bu-Lin Chen[a], Rui Zhang[b], Li Liu*[a], Xin-Xin Zhong*[a], Lei Wang*[b], Feng-Yan Li*[c], Guang-Hua Li[d], Khalid A. Alamry[e], Fa-Bao Li[a], Wai-Yeung Wong*[f], Hai-Mei Qin[g]

[a] *Hubei Collaborative Innovation Center for Advanced Organic Chemical Materials, Ministry of Education Key Laboratory for the Synthesis and Application of Organic Functional Molecules, School of Chemistry and Chemical Engineering, Hubei University, Wuhan 430062, P. R. China. E-mail: liulihubei@hubu.edu.cn; xxzhong@hubu.edu.cn*

[b] *Wuhan National Laboratory for Optoelectronics, Huazhong University of Science and Technology, Wuhan 430074, P. R. China. E-mail: wanglei@mail.hust.edu.cn*

[c] *Key Laboratory of Polyoxometalates Science of Ministry of Education, College of Chemistry, Northeast Normal University, Changchun, 130024, P. R. China. E-mail: lify525@nenu.edu.cn*

[d] *State Key Laboratory of Inorganic Synthesis and Preparative Chemistry, College of Chemistry, Jilin University, Changchun 130012, P. R. China.*

[e] *Chemistry Department, Faculty of Science, King Abdulaziz University, Jeddah 21589, Saudi Arabia*

[f] *Department of Applied Biology and Chemical Technology, The Hong Kong Polytechnic University, Hung Hom, Hong Kong, P. R. China. E-mail:* wai-yeung.wong@polyu.edu.hk

[g] *Fujian Provincial Key Lab of Theoretical and Computational Chemistry, and Department of Chemistry, College of Chemistry and Chemical Engineering, Xiamen University, Xiamen 361005, P. R. China.*

Ke Xu, Bu-Lin Chen and Rui Zhang contributed equally to this work.

Abstract

Highly emissive copper(I) halide nanoclusters having thermally activated delayed fluorescence (TADF) have been paid much attention, but rarely reported so far. Here, a hexanuclear copper(I) iodide cluster containing tridentate N^P^N ligand, $[Cu_6I_6(ppda)_2]$ {ppda = 2-[2-(dimthylamino)phenyl(phenyl)phosphino]-N,N-dimethylaniline}, was synthesized. All six copper atoms are four-coordinate, including four $CuPNI_2$ and two CuI_4 units. This complex exhibits intense white emission in powder state at room temperature and has peak wavelength at 535 nm (Φ_{PL} = 0.36) with microsecond lifetime (τ = 4.4 μs). Emission color can

be largely tuned from blue to white to yellow, from crystal to powder to film state at 297 K. The emission of $[Cu_6I_6(ppda)_2]$ originates from a combination of MLCT and XLCT transitions. This complex displayed good thermal stability. A solution-processed, nondoped device of complex $[Cu_6I_6(ppda)_2]$ exhibits stable yellow emission with CIE(x,y) of (0.43, 0.51). $[Cu_6I_6(ppda)_2]$ also shows a reasonable photocatalytic H_2 evolution activity under visible-light irradiation.

1. Introduction

Copper(I) complexes have been highly attractive due to the superiority in low cost, pro-environment, high brightness and facile luminescent modulation.[1] The low-lying MLCT excited states with small singlet-triplet energy gap facilitate Cu(I) complexes efficiently harvest triplet excitons for thermally activated delayed fluorescence (TADF) emission which potentially applied in highly efficient organic light-emitting diodes (OLEDs).

Cu(I) complexes usually have a distorted tetrahedral geometry around the Cu atom, which often exhibit relatively low quantum yield due to increased non-radiative decay.[2] To overcome the problem, one way is using the trigonal-planar structure with rigid ligands[3] or two-coordinate Cu(I) complex[4] to hamper the Jahn-Teller distortion, a signifcant example was reported by Osawa and co-workers, a highly efficient, green, three-coordinate Cu(I) halide with a EQE over 20%. Another way is to design a firm framework with bulky or bridged ligands.[3,5] A highly emissive, yellow, four-coordinate mononuclear Cu iodide complex using a tridentate phosphine ligand with a EQE of 16.3%, and negligible roll-off was made by Xu's group.[6]

In comparison to mono- and dinuclear Cu(I) complexes (n = 1, 2),[7-14] nanoclusters (n ≥ 3)[15-18] have advantages of rigidity, and therefore thermo- and photostability. However, only one Cu_4I_4 cluster was used as emitter in OLED to date.[19] The main challenge is their poor processability and weak eletroactivities.

Based on the high luminescence efficiency of the Cu(I) halide complexes,[20-26] a rigid/congested structure is important to avoid structural changes in the excited state. For this reason, a N^P^N tridentate ligand, 2-[2-(dimthylamino)phenyl(phenyl)phosphino]-N,N-dimethylaniline is employed, likely obtain high efficiency emissive Cu(I) complex. Reported here is a luminescent four-coordinate copper(I) iodide cluster, the molecular structure and photophysical and photocatalytic properties are investigated.

2. Experimental

2.1. Materials

All reagents and solvents are of commercial reagent grade and used without further purification except where noted. Tetrahydrofuran (THF) was distilled under nitrogen in the presence of sodium chips using benzophenone ketyl as an indicator. 2-bromo-*N*,*N*-dimethylaniline was synthesized according to the literature method.[27]

2.2. Instrumentation

^1H, ^{13}C and ^{31}P NMR spectra were recorded on a Varian 600 or 400 MHz NMR spectrometer using deuterated solvents as the lock and reference. Chemical shifts were reported in ppm relative to $SiMe_4$ for the ^1H and 85% H_3PO_4 for the ^{31}P nucleus. High-resolution mass spectra

reported as *m/z* were obtained on a Bruker Autoflex MALDI-TOF mass spectrometer. C and H analyses were determined using a Vario Micro Cube elemental analyzer. The single crystal structure of the complex $[Cu_6I_6(ppda)_2]$ was measured at room temperature using Bruker P4 Venture diffractometer. The powder X-ray diffraction data were obtained from a Bruker-D8 Advance diffractometer. UV–vis spectra were recorded on a Unicam Helios α spectrometer. Photoluminescence spectra were recorded on a FLS920 steady state & time-resolved fluorescence spectrometer. Solid-state Φ_{PL} values were determined using a Hamamatsu system for absolute PL quantum yield measurements equipped with an integrating sphere with Spectralon inner surface coating. The PL lifetimes were measured by a single photon counting spectrometer from Edinburgh Instruments (FLS920) with a Picosecond Pulsed UVLASTER (LASTER377) as the excitation source. The samples were carefully degassed by at least five freeze-pump-thaw cycles. Thermogravimetric analysis (TGA) was performed on a Perkin-Elmer Diamond TG/DTA thermal analyzer. The elemental composition was determined with SEM/EDS (Hitachi SU-800 FE-SEM). The hydrogen evolved was analyzed with a gas chromatograph (Agilent 6890GC, thermal conductivity, Ar carrier).

2.3. Syntheses

2.3.1. Synthesis of 2-[2-(dimthylamino)phenyl(phenyl)phosphino]-N,N-dimethylaniline (ppda)

n-BuLi (2.5 M in hexane, 2 mL, 5 mmol) was added dropwise to a solution of 2-bromo-*N*,*N*-dimethylaniline (1 g, 5 mmol) in THF/Et_2O (1:1, 20 mL) at −110°C, the reaction mixture was stirred at −110°C for 5 min. $PhPCl_2$ (0.34 mL, 2.5 mmol) was added

during 5 min. The resulted pale yellow solution was gradually warmed to room temperature and stirred for 8 h. The reaction was then quenched by addition of water (10 mL). The mixture was treated with aqueous NH_4Cl and extracted with CH_2Cl_2 (3×10 mL). The extracts were combined and dried over anhydrous Na_2SO_4. After removal of solvent, the residue was purified by flash chromatography to afford the white powder of 0.436 g with a yield of 50%. ^{1}H NMR (600 MHz, $CDCl_3$): δ: 7.32-7.26 (m, 5H), 7.21-7.17 (m, 4H), 6.96 (t, J = 6 Hz, 2H), 6.81-6.78 (m, 2H), 2.63 (s, 12H). ^{13}C NMR (100 MHz, d_6-DMSO), δ = 157.45, 138.92, 134.93, 133.58, 133.07, 129.70, 128.21, 127.97, 124.09, 120.31, 44.97. ^{31}P NMR (200 M, $CDCl_3$) δ: −17.45 (s). Anal. Calcd for $C_{22}H_{25}N_2P$: C, 75.84; H, 7.23; N, 8.04. Found: C, 75.90; H, 7.18; N, 8.09. MS (MALDI-TOF): *m/z* calcd for $[C_{22}H_{25}N_2P+H]^+$, 349.1755, found: 349.1767.

2.3.2. Synthesis of $[Cu_6I_6(ppda)_2]$

A suspension of copper(I) iodide (0.057 g, 0.30 mmol) and ppda (0.105 g, 0.30 mmol) in 30 mL of CH_3CN was stirred for 3 days at room temperature to form a white precipitate. The precipitate was filtered off, and $[Cu_6I_6(ppda)_2]$ was crystallized from the filtered solution after slow evaporation at room temperature to give colorless crystals of 0.066 g with a yield of 72%. ^{1}H NMR (600 MHz, $CDCl_3$) δ: 7.84-7.76 (m, 2H), 7.68-7.55 (m, 6H), 7.47-7.39 (m, 12H), 7.20-7.15 (m, 6H), 2.67 (s, 24H). ^{31}P NMR (200 M, $CDCl_3$) δ: −31.73. Anal. Calcd for $C_{44}H_{50}Cu_6I_6N_4P_2$: C, 28.73; H, 2.74. Found: C, 28.77; H, 2.71. MS (MALDI-TOF): *m/z* calcd for $[Cu_2I(dppa)+H]^+$, 601.9392, found: 601.3938. A solution of $[Cu_6I_6(ppda)_2]$ crystals dissolved in CH_3CN was evaporated to remove organic solvent under vacuum, a powder

sample is obtained. Anal. Calcd for $C_{44}H_{50}Cu_6I_6N_4P_2$: C, 28.73; H, 2.74. Found: C, 28.78; H, 2.73. A solution of $[Cu_6I_6(ppda)_2]$ dissolved in CH_3CN (10 mg/mL) was spin coated onto the substrate at 2000 r.p.m for 50 s, a film sample is obtained.

2.4. X-ray crytallography

Colorless crystals of complex $[Cu_6I_6(ppda)_2]$ suitable for X-ray diffraction study were grown by slow evaporation of its solution in acetonitrile at room temperature. Geometric and intensity data were collected using graphite-monochromated Mo Kα radiation (λ = 0.71073 Å) on a Bruker AXS APEX II CCD area detector. The collected frames were processed with the software *SAINT*[28], and an absorption correction was applied (*SADABS*)[29] to the collected reflections. The structures were solved by direct methods (*SHELXTL*)[30] in conjunction with standard difference Fourier techniques and subsequently refined by full-matrix least-squares analyses on F^2. All non-hydrogen atoms were assigned with anisotropic displacement parameters.

2.5. Theoretical calculations

The structural parameters for complex $[Cu_6I_6(ppda)_2]$ were obtained from the crystal data which are listed in Tables 1 and 2. The ground-state (S_0) geometry was then optimized at theoretical level of B3LYP-D3(BJ)/6-311+G(d,p) (LANL2D2 for Cu and I atoms), where D3(BJ) was Grimme's D3 dispersion correction with Becke-Jonson damping. To calculate the adiabatic excitation energies, the optimized geometries of S_1 and T_1 are required, which were obtained at theoretical levels of TD-B3LYP-D3(BJ)/6-31+G(d) and UB3LYP-D3(BJ)/6-31+G(d) (LANL2D2 for Cu and I atoms), respectively. The absorption

spectrum based on the optimized S_0 geometry was obtained at the TD-B3LYP-D3(BJ)/6-311+G(d,p) (LANL2D2 for Cu and I atoms) level. In addition, the solvent effect was taken into account by the polarizable continuum model (PCM, solvent=acetonitrile) for the purpose of comparing with the experimental spectrum. All the calculations were manipulated by the Gaussian 16 suite.[31]

Table 1. Crystallographic data and details for $[Cu_6I_6(ppda)_2]$

	$[Cu_6I_6(ppda)_2]$
Empirical formula	$C_{44}H_{50}Cu_6I_6N_4P_2$
Formula weight	1839.46
Temperature (K)	293(2)
Wavelength (Å)	0.71073
Crystal system	Monoclinic
Space group	P2(1)/n
a (Å)	12.7527(40)
b (Å)	13.5827(38)
c (Å)	15.2564(41)
V (Å^3)	2637.9(9)
Z	2
ρ (g cm^{-3})	2.316
μ (mm^{-1})	5.982
F (0 0 0)	1728
θ range for data collection (°)	3.00 to 27.47
Index ranges	$-16 \le h \le 16$
	$-17 \le k \le 17$
	$-19 \le l \le 19$
Independent reflections	24543 [*R*(int) = 0.0953]
Completeness to θ = 25.242°	99.4 %
Max. and min. transmission	0.3478 and 0.2864
Gof	1.082
Final *R* indices [$I > 2\sigma(I)$]	R_1= 0.0536
	wR_2= 0.1263
R (all data)	R_1= 0.0598
	wR_2= 0.1304
Max/min (e Å^3)	2.772 and −2.281

Table 2. Selected bond lengths [Å] and angles (°) for $[Cu_6I_6(ppda)_2]$

	$[Cu_6I_6(ppda)_2]$

Cu–I	2.5854(9) , 2.6067(10), 2.6287(8), 2.6947(11), 2.6756(10), 2.6461(12), 2.7664(10), 2.7782(11)
Cu–P	2.3447(14) , 2.5008(15)
Cu–N	2.098(4), 2.121(5)
Cu···Cu	2.4135(13), 2.7424(11), 2.8334(11), 3.0259(18)
I–Cu–I	104.16(3), 105.48(3), 107.66(3), 108.01(4), 108.06(3), 111.41(4), 114.73(3), 116.98(4)
Cu–I–Cu	53.14(3), 61.29(2), 61.46(2), 62.00(2), 65.57(3), 68.59(4), 120.66(3)
I–Cu–N	106.68(12), 109.12(13), 110.70(12), 116.37(13)
I–Cu–P	106.95(5), 116.95(4), 117.96(5), 131.75(4)
P–Cu–N	83.66(13), 86.51(12)
Cu–P–Cu	59.65(4)

2.6. Device Fabrication

Patterned indium tin oxide (ITO) glass substrates with the sheet resistance less than 15 Ω/sq were successively cleaned with alkaline cleaner diluted with deionized water, acetone and isopropanol by ultrasonic cleaning and then oven-dried for more than 3 hours after quick drying with N_2. The ITO glass substrates were then treated with the oxygen plasma for 5 min in air. Poly(3,4-ethylenedioxythiophene)/poly(styrenesulfonate) (PEDOT: PSS) solutions (Baytron PVP Al 4083, filtered through a 0.22 μm filter) were spin-coated onto the ITO-coated glass substrates at the speed of 2000 r.p.m. for 50 s and baked at 120 ºC for 30 min in the air. The PEDOT: PSS-coated substrates were transferred into a nitrogen-filled glove box (O_2 < 1p.p.m., H_2O < 1p.p.m.). Then a solution of $[Cu_6I_6(ppda)_2]$ dissolved in DMF (15 mg/mL) was spin coated onto the substrates at 2000 r.p.m for 50 s and baked at 100 ºC for 10 min in the glove box to volatilize the DMF and acquire a smooth film of emitting layer (EML) material. Finally, the substrates were transferred to a vacuum chamber and after that

1,3,5- tris(1-phenyl-1H-benzimidazole-2-yl)benzene (TPBi, 30 nm) and LiF/Al electrodes (1 nm/100 nm) were deposited using a thermal evaporation system through a shadow mask under a high vacuum of $\approx 4 \times 10^{-4}$ Pa. The current density-voltage and luminance-voltage were measured using a Keithley 2400 source measurement unite and in the meanwhile the efficiency was measured with a PhotoResearch spectroradiometer (PR655), and all the tests were conducted in the air without encapsulation.

2.7. Photocatalytic hydrogen production

The photocatalytic hydrogen production test was performed in a closed system with a 200 mL quartz flask at room temperature. A 300 W xenon lamp (Beijing Perfectlight Technology Corp., China) was used as the light source with an AM 1.5 optical filter and photocurrent density was 100 mW cm^{-2}. In a typical photocatalytic experiment, 50 mg of the prepared photocatalyst ($Cu_6I_6(ppda)_2$ in powder state) was suspended in 200 mL mixed solution containing CH_3OH (20 vol%) as sacrificial reagents and DI water. Nitrogen was purged through the cell for 30 minutes to remove oxygen before photocatalytic reaction. The blank experiments showed no appreciable hydrogen evolution in the absence of irradiation or photocatalyst. After a continuous reaction for 3h, the photocatalyst was centrifuged and redispersed in a new reaction solution with fresh sacrificial reagents.

3. Results and discussion

3.1. Description of syntheses and structures

The synthetic routes for ligand ppda and complex [$Cu_6I_6(ppda)_2$] are outlined in Scheme 1. First, methyl iodide was used to methylate the 2-bromoaniline to furnish

2-bromo-*N*,*N*-dimethylaniline in 70% yield. Then the synthesis of 2-dimethylaminophenyllithium was carried out in a mixture with the mole ratio of 1:1 for 2-bromo-*N*,*N*-dimethylaniline and *n*-butyllithium. By the addition of dichlorophenylphosphine to 2-dimethylaminophenyllithium in THF at −110 °C under nitrogen, ppda was synthesized in 50% yield. Complex $[Cu_6I_6(ppda)_2]$ was prepared by mixing a suspension of CuI in acetonitrile with 1 equivalent of ppda. A new hexanuclear Cu(I) iodide complex was obtained as air stable crystal in high purity and found to be generally soluble in acetonitrile, methanol, chloroform and DMF. It was characterized by MALDI-TOF spectrometry, single crystal X-ray diffraction, and NMR spectroscopy and gave satisfactory analytical data.

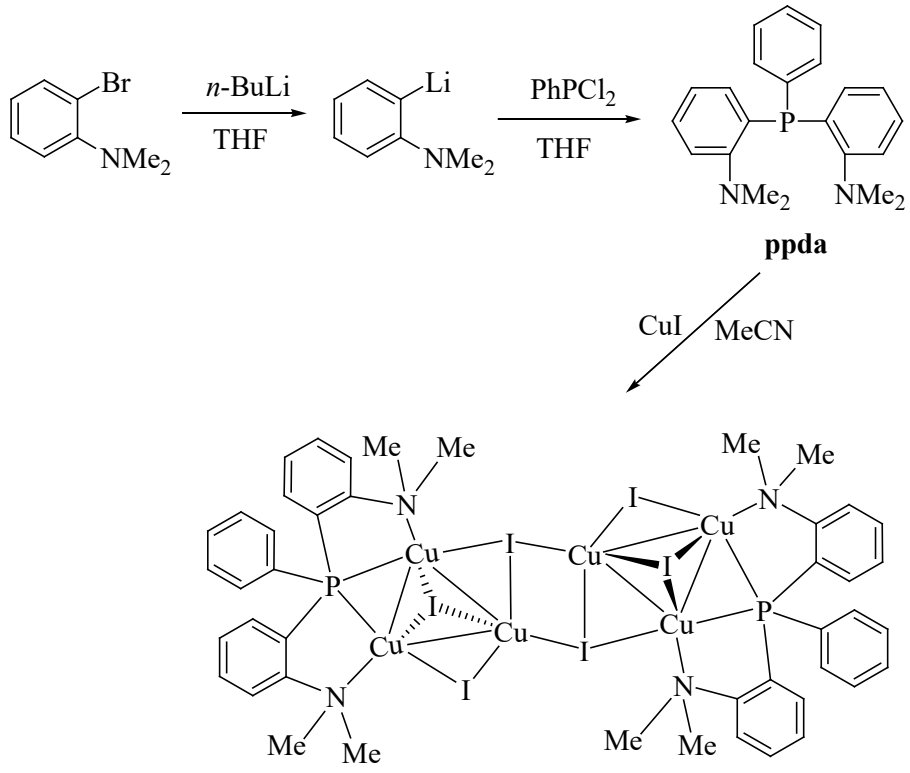

$[Cu_6I_6(ppda)_2]$

Scheme 1. Synthetic pathways to ligand ppda and complex $[Cu_6I_6(ppda)_2]$.

3.2. X-ray crystallographic study

Perspective view of complex $[Cu_6I_6(ppda)_2]$ is shown in Fig.1. Crystallographic data and selected bond lengths and angles are given in Tables 1 and 2, respectively. X-ray crystallographic study on complex $[Cu_6I_6(ppda)_2]$ reveal a hexanuclear Cu_6I_6 cluster, in which four Cu atoms are involved in tetrahedral geometries and each Cu atom is coordinated by two iodide atoms and a nitrogen and a phosphor atoms from the ppda ligand. The remaining two Cu atoms are in tetrahedrally coordinated by four iodide atoms. The distances of Cu-I bonds are from 2.5854 to 2.7782, which are within the normal ranges as the data reported before.[32] The average Cu-N distance is 2.1095 Å, slightly shorter than those observed in $[Cu(\mu\text{-}I)(PNMe_2)]_2$ (2.250 and 2.232 Å),[25] reflecting the enhanced coordination strength. Accordingly, the distances of Cu–P are from 2.3447 to 2.5010 Å, which are longer than those observed in $[Cu(\mu\text{-}I)(PNMe_2)]_2$ (2.210 and 2.213 Å),[25] displaying the highly congested environment around phosphorus atoms. Two copper(I) centers (Cu3 and Cu3') are bridged by two iodide atoms (I2 and I2') with a planar four-membered Cu_2X_2 ring. The centroid of the $Cu_3I_2Cu_3'I_2'$ ring is also the centre of symmetry of the complex, with two iodide atoms (I1 and I1') take on the trigonal pyramidal geometries symmetrically. It is noted that the metallophilic interactions exist in two trigonal pyramidal geometries, with the Cu⋯Cu distances (2.4135 Å for $Cu_1\cdots Cu_2$ and $Cu_1'\cdots Cu_2'$, 2.7424 Å for $Cu_3\cdots Cu_2$ and $Cu_3'\cdots Cu_2'$) shorter than the van der Waals distance (2.80 Å), and weaker Cu⋯Cu interactions for $Cu_1\cdots Cu_3$, $Cu_1'\cdots Cu_3'$ (2.8334 Å) and $Cu_3\cdots Cu_3'$ (3.0259 Å). Furthermore, complex $[Cu_6I_6(ppda)_2]$ has an elliptical configuration with diameters of 1.7 and 2.0 nm (Fig.S6), making it competent as a nanoemitter for super-resolution display. Intermolecular hydrogen

bonds can be observed in $[Cu_6I_6(ppda)_2]$, with the closest H-to-I distance of 3.120 Å. Complex $[Cu_6I_6(ppda)_2]$ also shows the intermolecular C-H···π interactions between phenyl rings with the closest C-to-H distance of 2.760 Å. Overall, all these intermolecular interactions are incorporated into 2-D sheet for complex $[Cu_6I_6(ppda)_2]$ (Supporting Information Fig.S7).

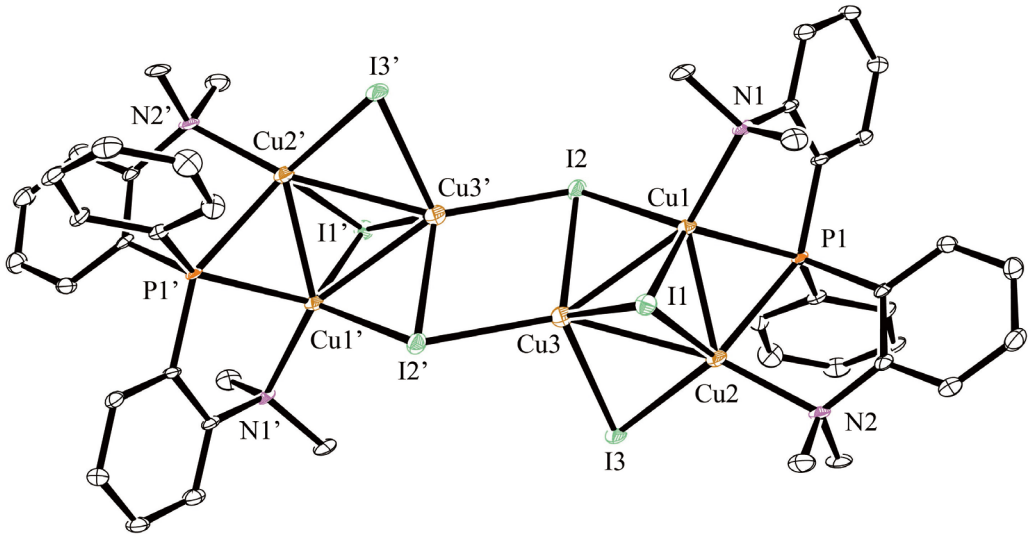

Fig.1. ORTEP diagram of complex $[Cu_6I_6(ppda)_2]$, H atoms were omitted for clarity.

3.3. Photophysical properties and theoretical calculations

The absorption spectra of complex $[Cu_6I_6(ppda)_2]$ and ppda in CH_3CN (5.5×10^{-6} M) at room temperature are shown in Fig.2. The absorption spectrum of ppda exhibits a broad, intense band at 211 nm ($\varepsilon = 2.80 \times 10^4$ M^{-1} cm^{-1}), which is characteristic of an aryl phosphine and amine compound. This band is assigned to a mixed transition of n–π* and π–π*; the former one involves the transition of an electron from the lone pair orbital on phosphorus or nitrogen to an empty antibonding π* orbital on a phenyl ring and the latter is the electron transition from a phenyl ring to the same or another phenyl ring. Complex $[Cu_6I_6(ppda)_2]$ has

an intense absorption band with a maximum at 245 nm [$\varepsilon = 1.87 \times 10^4$ M^{-1} cm^{-1}] and a weaker band tail at 280–350 nm. The weaker band tail may be attributed to the electronic transition being affected by the copper ions, the halide ligands, or both, or intraligand charge transfer ($n \rightarrow \pi^*$, $\pi \rightarrow \pi^*$ or both). The absorption spectrum of complex $[Cu_6I_6(ppda)_2]$ in CH_3CN from our TDDFT calculations is shown in Fig.S18 in supporting information, which is consistent with the experimental data. According to the excitation properties (Table S2, Fig. S19) for complex $[Cu_6I_6(ppda)_2]$, the main contributions to the lowest excited state are identified as the mixed transitions from HOMO (highest occupied molecular orbital) and HOMO−1 to LUMO+1 (LUMO: lowest unoccupied molecular orbital). As shown in Fig.3, the contour plots of HOMO−1, HOMO and LUMO+1 at optimized S_0 geometry reveal that the electrons in HOMO and HOMO−1 are mainly distributed over the copper and halogen atoms, while the holes in LUMO+1 are mainly localized on the phenyl rings of ppda. We can thus conclude that the lowest excited state of $[Cu_6I_6(ppda)_2]$ (280–350 nm) consists of metal-to-ligand charge transfer (MLCT) and halogen-to-ligand charge transfer (XLCT) state transition, analogous to those in Cu(I) halides complexes containing di- and tri-phosphine ligand such as $[CuI(dppb)(PPh_3)]$ and TTPPCuX.[21-23,33]. We also measured the UV-Vis absorption spectra of $[Cu_6I_6(ppda)_2]$ in CH_3CN with the concentration range from 2.0×10^{-5} to 2.5×10^{-7} M (Fig.S9). The concentration dependence of the absorption intensity follows Beer's law, which confirms the solution stability and indicates the maintaining of the hexanuclear cluster structure.

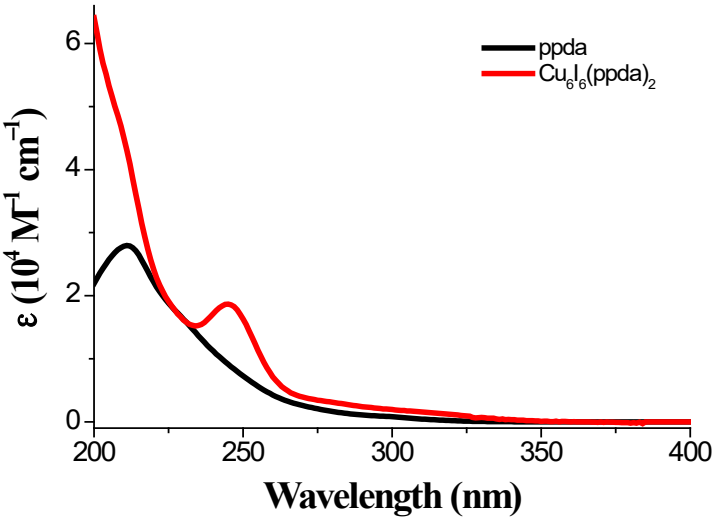

Fig.2. Absorption spectra of ppda and complex $[Cu_6I_6(ppda)_2]$ in CH_3CN at 297 K.

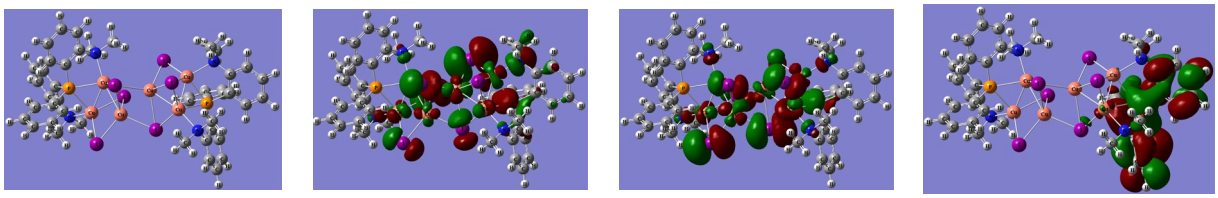

The optimized S_0 geometry	HOMO−1 E = –5.90 eV	HOMO E = –5.79 eV	LUMO+1 E = –1.48 eV

Fig.3. The optimized S_0 geometry, electron cloud distribution of HOMO−1, HOMO and LUMO+1 for complex $[Cu_6I_6(ppda)_2]$.

The emission spectra of complex $[Cu_6I_6(ppda)_2]$ in crystal and powder state measured at 297 K and 77 K are shown in Fig.4 and the emission maxima, lifetimes and quantum yields of the complex at 297 K and 77 K are summarized in Table 3. Complex $[Cu_6I_6(ppda)_2]$ in crystal state shows intense blue emission at 476 nm (λ_{ex}= 372 nm, τ = 2.7 μs, Φ_{PL} = 0.0035 in air) with a weaker shoulder at 420 nm, and a relatively weak low energy emission at 716 nm (τ = 73.3 ns). In powder state it shows intense white emission at 535 nm (λ_{ex}= 350 nm, Φ_{PL} = 0.36 in vacuum) with a weaker shoulder at 450 nm. The weaker shoulder emission at 450 nm in

powder state is from the ligand ppda when compared with the emission of ligand ppda in powder state at 297 K (Fig.S16). In film state, the emission color changes to yellow with wavelength maxima at 563 nm and a much weaker peak at 415 nm. From crystal to powder to film state, structural relaxation should take place at 297 K, rending a bathochromic shift to the emission ($\lambda_{em}^{crystal} = 476 \rightarrow \lambda_{em}^{powder} = 535 \rightarrow \lambda_{em}^{film} = 563$ nm). The PXRD patterns of the powder and film samples confirm some structural changes in the crushed state and large changes in amorphous state when compared to the simulated peaks from the single-crystal data (Fig.S8). Much lower quantum yield of complex $[Cu_6I_6(ppda)_2]$ in crystal state than that in powder state under vacuum, the main reason is due to the reduction of intermolecular interaction-induced quenching through the transformation from crystal to powder state as evidenced by powder X-ray diffraction analysis, analogous to copper iodide nanocluster $[DBFDP]_2Cu_4I_4$[19]. Based on the PL data in crystal, powder and film state at 297 K, the Commission Internationale de L'Eclairage color coordinates are (0.2278, 0.2784), (0.2938, 0.3707) and (0.3990, 0.4613), respectively (Fig.5). The CIE value for the powder state is quite near to the saturated white point of (0.33, 0.33). As far as we know, this is the first report on efficient white light and the nearest to saturated white emission from neutral Cu(I) halide complexes and the PLQY is the highest among Cu(I) halide clusters.

The emission properties of complex $[Cu_6I_6(ppda)_2]$ were also estimated based on the optimized S_1 geometries using the TDDFT method. The calculated emission wavelength of complex $[Cu_6I_6(ppda)_2]$ (Table 3) suggests the reliability of our TDDFT method as the theoretical value (463 nm) agrees well with the experimental one (476 nm). The

LUMO⇒HOMO transition is identified as the main contribution to the emission; the contour plots of the HOMO and LUMO based on the S_1 state geometry are in Fig.6. The LUMO is mainly from Cu and X, and the HOMO is mainly confined to the phenyl rings in ppda. These indicate that the luminescence mainly arises from XLCT and MLCT transitions.

At 77 K, the emission maxima of complex $[Cu_6I_6(ppda)_2]$ is located at 470 nm both in the crystal and powder states. A relatively weak emission at 711 nm is observed in the crystal state, similar as it at 297 K (716 nm), which may be from the difference of structures between the crystal and powder. We analyzed the effect of molecular aggregates on the emission spectra through the electronic structure calculations using TDDFT method. Owing to hundreds of atoms, the optimized geometries of S_1 and T_1 cannot be obtained. However, the absorption spectra of one, two and three molecules based on the crystal data were calculated to present the effect of molecular aggregates. The results (Supporting Information Table S3) showed that the absorptions at 297 K and 77 K are both red-shifted with the number of molecules increasing, therefore, we can conclude that the molecular aggregates will result in the emissions at 716 nm and 711 nm of the crystal. The molecular aggregates are possibly ascribed to the intermolecular hydrogen bonds (H-to-I) and intermolecular C-H⋯π interactions between phenyl rings which are discussed in X-ray crystallographic study. The excitation spectrum with emission wavelength at 716 nm of complex $[Cu_6I_6(ppda)_2]$ in crystal state is quite different from that with emission wavelength at 474 nm, indicating different emission origin at 474 and 716 nm (Fig.S15). The intense, longer excitation wavelength at 404 nm is possibly due to the the molecular aggregates. In addition, the emission lifetime at

716 nm of complex $[Cu_6I_6(ppda)_2]$ in crystal state is very short (73.3 ns), which might support the molecular aggregates as well. The emission bands (470 and 711 nm) at 77 K are blue-shifted in comparison to the bands (476 and 716 nm) at 297 K upon cooling possibly due to suppression of the excited state energy relaxation caused by structural changes involving vibrations and rotations.[20]

The S_1 and T_1 energy levels of 3.3244 and 3.2208 eV are estimated according to the emission peak onsets at 297 K and 77 K (Fig.S17). The resulted $\Delta E(S_1\text{-}T_1)$ of 0.1036 eV is very small to make RISC feasible. We found that the lifetime of luminescence from the solid state at 297 K is 2 orders of magnitude shorter than those at 77 K, which is also consistent with the TADF mechanism.[25,34] Fig.7 shows the temperature dependence of the decay times in the solid state for the complex. In the temperature range between 77 and 317 K, the decay is two-exponential. At 77 K, the emissive state is dominated by the lowest triplet state (T_1). The corresponding transition has long decay time because the transition from the lowest triplet state to the singlet ground state is spin-forbidden. With the temperature increase, a strong reduction of the emission decay time is observed. The thermal activation of the short-lived singlet state S_1 that decay irradiatively to give the TADF, is evidenced.

The radiative rate constant k_r of complex $[Cu_6I_6(ppda)_2]$ was calculated to be 8.18×10^4 s^{-1} in powder state, and 1.33×10^3 s^{-1} in crystal state at 297 K, respectively. The value in powder state is similar with those Cu(I) halide containing tridentate phosphine complex TTPPCuX [22b], and copper iodide nanocluster $[DBFDP]_2Cu_4I_4$[19]. Copper iodide nanocluster $[DBFDP]_2Cu_4I_4$ in crystal state is nonluminous[19].

The selected bond lengths and angles in the optimized S_0, and S_1 geometries for complex $[Cu_6I_6(ppda)_2]$ are collected in Table S1. The S_1 coordination geometries of the copper center of $[Cu_6I_6(ppda)_2]$ are highly distorted tetrahedral, with I-Cu-N, I-Cu-P, P-Cu-N and Cu-P-P bond angles essentially unchanged in comparison to the ground state (S_0) due to the rigid structure of tridentate ligand ppda. Some changes are observed in I-Cu-I and Cu-I-Cu bond angles, which possibly results in some nonradiative processes cause by Jahn-Teller distortion of emissive excited states[3] and not very high quantum efficiency. Structural relaxation in I-Cu-I and Cu-I-Cu bond angles possibly results in a bathochromic shift to the emission, from crystal to powder to film state at 297 K.

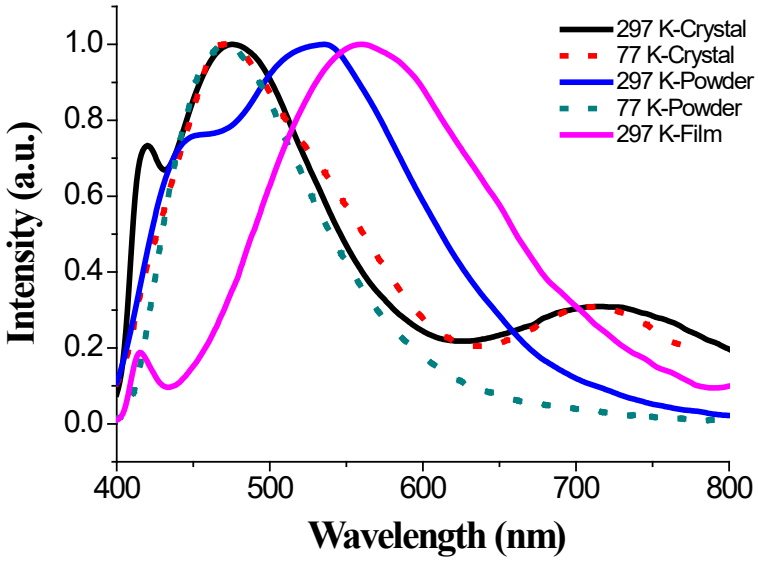

Fig.4. Normalized emission spectra of $[Cu_6I_6(ppda)_2]$ in crystal state at 297 K (λ_{ex} = 372 nm) and 77 K (λ_{ex} = 350 nm), in powder state at 297 K (λ_{ex} = 350 nm) and 77 K (λ_{ex} = 320 nm) and in film state (λ_{ex} = 370 nm)

Table 3. Photophysical data of $[Cu_6I_6(ppda)_2]$ in the solid state.

	λ_{max} (nm)[a]		τ (μs)[b]		Φ[c]		k_r[d] ($10^4 s^{-1}$)	λ (nm)[e]
$[Cu_6I_6(ppda)_2]$	297 K	77 K	297 K	77 K	297 K	77 K		
Crystal	476	470	2.7	214	0.0035 (0.0036*)	/	0.133*	463

Powder	535	470	4.4	717	0.36*	0.73*	8.18*
Film	563				0.15		

[a] Emission peak wavelength in crystal and powder state.

[b] Average lifetime was used and calculated by the equation $\tau_{ave} = \Sigma B_i T_i^2 / \Sigma B_i T_i$, B_i and T_i are are shown in Figures S8-S12. Experimental errors are ± 5%.

[c] Absolute emission quantum in crystal in air, asterisk indicates under vacuum. Experimental errors are ± 5%.

[d] Radiative decay rate constant in crystal and powder state. $k_r = \Phi/\tau_{ave}$.

[e] Calculated emission wavelengths based on the optimized S_1 geometries.

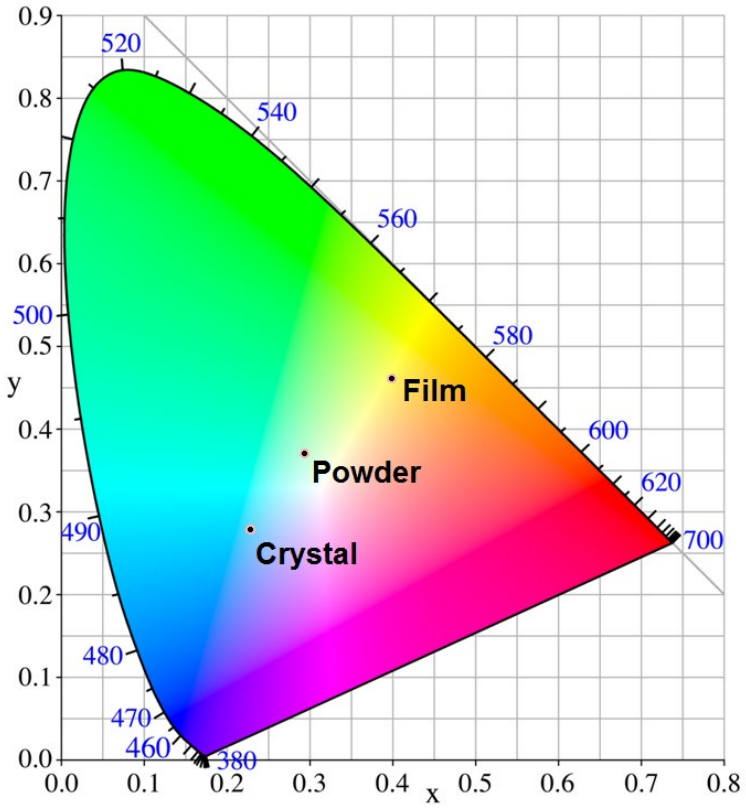

Fig. 5. CIE graph of complex $[Cu_6I_6(ppda)_2]$ in crystal, powder and film state.

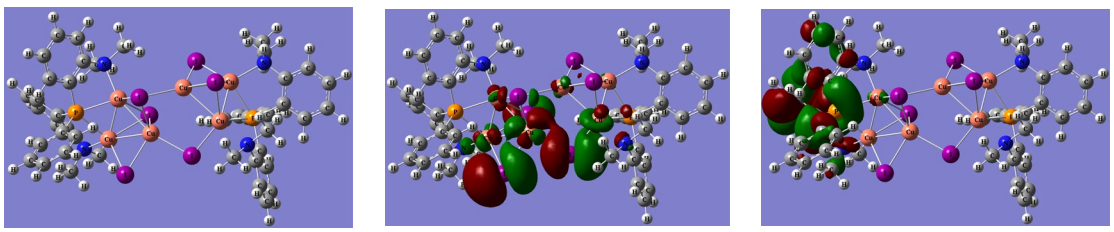

The optimized S_1 geometry HOMO E = –4.58 eV LUMO E = –2.11 eV

Fig.6. The optimized S_1 geometry, electron cloud distribution of HOMO and LUMO at S_1 geometry for complex $[Cu_6I_6(ppda)_2]$.

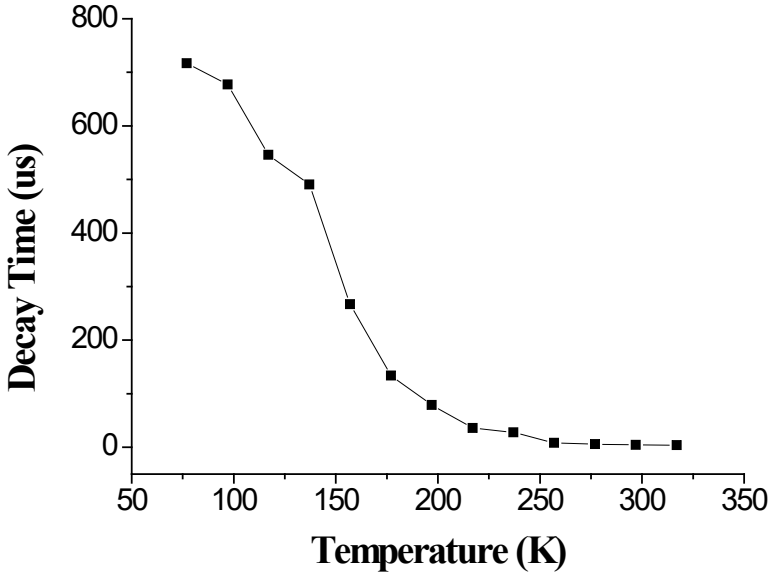

Fig.7. Temperature dependence of decay time for complex $[Cu_6I_6(ppda)_2]$ in powder state.

3.4. Thermal properties

Since good thermal stabilities of the complexes are important for OLED applications, the onset decomposition temperature (T_{dec}) of $[Cu_6I_6(ppda)_2]$ was determined by thermogravimetric analysis (TGA) under a stream of nitrogen. From the onset of the TGA curve (Fig.8), $[Cu_6I_6(ppda)_2]$ shows good thermal stability with its T_{dec} value at 248 °C with weight loss of ca. 2%. The first-step weight loss for the complex $[Cu_6I_6(ppda)_2]$ of ca. 21% was observed at 395 °C, which is due to the removal of two I atoms and eight methyls from two ppda. The second-step weight loss was observed at 524 °C, which is ascribed to the removal of four I atoms and further decomposition of two ppda ligands.

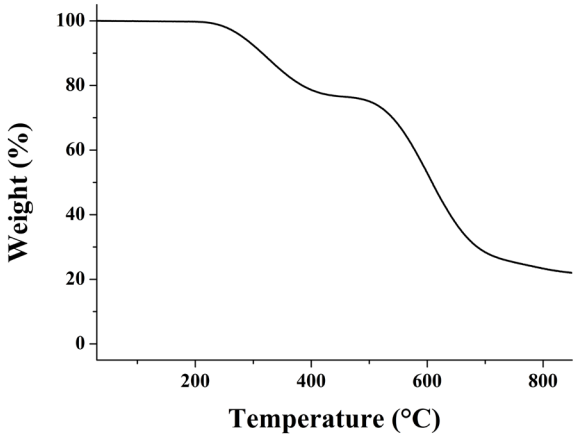

Fig.8. TGA trace of complex $[Cu_6I_6(ppda)_2]$.

3.5 Electroluminescent properties

The solution-processed devices based on complex $[Cu_6I_6(ppda)_2]$ were fabricated with the structure of ITO/ PEDOT:PSS (40 nm)/ complex $[Cu_6I_6(ppda)_2]$ (40 nm)/ TPBi (30 nm)/ LiF (1 nm)/ Al (100 nm). In the device, ITO (indium tin oxide) was used as the anode, PEDOT: PSS (Poly(3,4-ethylenedioxythiophene)：poly(styrenesulfonate)) used as hole injection and hole transport layer, complex $[Cu_6I_6(ppda)_2]$ used as the EML, 1,3,5-Tris(1-phenyl-1H-benzimidazol-2-yl)benzene (TPBi) used as the electron transport layer, LiF served as electron injection layer and Al as cathode. The energy-level diagram of the device is shown in Fig.9(a). This device exhibits yellow emission at 564 nm with CIE (x, y) of (0.43, 0.51). The EL spectrum of the device is shown in Fig.9(b). The device gives maximum external quantum efficiency (EQE) of 0.31% and presented maximum current efficiency (CE) of 0.85 cd/A. The performance of the device is less satisfactory than we expected. We speculate the energy levels don't match up very well and further work should be made to find more suitable transporting materials for $[Cu_6I_6(ppda)_2]$. In addition, we have

tried CBP (4,4'-bis(carbazol-9-yl)biphenyl), DPEPO (bis{2-[di(phenyl)phosphino]phenyl}etheroxide), mCP (N,N-dicarbazolyl-3,5-benzene) and mCBP (3,3-di(9H-carbazol-9-yl)biphenyl) as the host materials, and complex $[Cu_6I_6(ppda)_2]$ as the emitter to fabricate doped devices to improve the luminescence performance of OLED devices. However, we found that due to the limited solubility of the complex $[Cu_6I_6(ppda)_2]$, the solvent DMF or DMSO used could not dissolve the above host materials. Then we also came up with a way to use mixed solvents by dissolving the complex $[Cu_6I_6(ppda)_2]$ in DMF or DMSO accompanied with dissolving host material mCBP in acetone, and then mixing to prepare the doped device. Due to the different evaporation rates of the two solvents, the quality of the film is poor, which results in OLED device without emitting light.

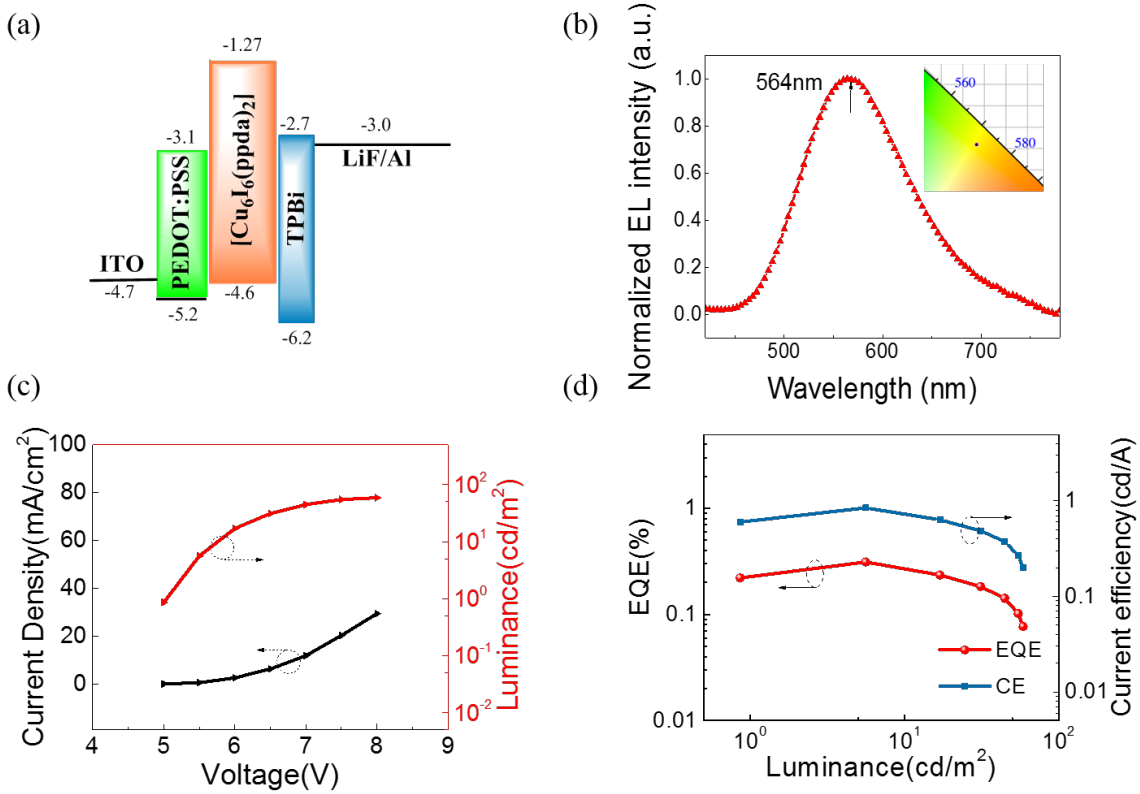

Fig.9. (a) Energy-level diagram of the device based on $[Cu_6I_6(ppda)_2]$; (b) the EL spectra of the device at 5V, and the inset is the corresponding CIE; (c) current density–voltage–luminance (J–V–L) characteristics; (d) EQE–luminance and CE–luminance characteristics.

3.6 Photocatalytic properties

The photocatalytic H_2 evolution experiments were carried out using complex $[Cu_6I_6(ppda)_2]$ as the light photosensitizer and photocatalyst. Methanol was employed as a sacrificial electron donor, being the source of the electrons required in the reduction semi-reaction of water. The photocatalytic activity of complex $[Cu_6I_6(ppda)_2]$ could be recovered owing to the re-exposed active-sites and the renewed sacrificial reagents. As shown in Fig.10, the H_2 evolution rate of complex $[Cu_6I_6(ppda)_2]$ was 22.30, 21.67 and 20.00 μmol/h, respectively. The total amount of evoluted H_2 during 9h was 191.9 μmol, which demonstrates that complex $[Cu_6I_6(ppda)_2]$ shows photocatalytic H_2 evolution activity under visible-light irradiation. The activity of the photocatalyst is presumably attributed to the enhanced visible light harvesting of complex $[Cu_6I_6(ppda)_2]$ and the effective electron-hole separation in the complex. SEM-EDS for the Cu_6I_6 cluster was exhibited in Fig.S20 before and after the photocatalysis. The atom (%) have no obviously change, which indicated that the Cu_6I_6 cluster undecomposed during the photocatalysis.

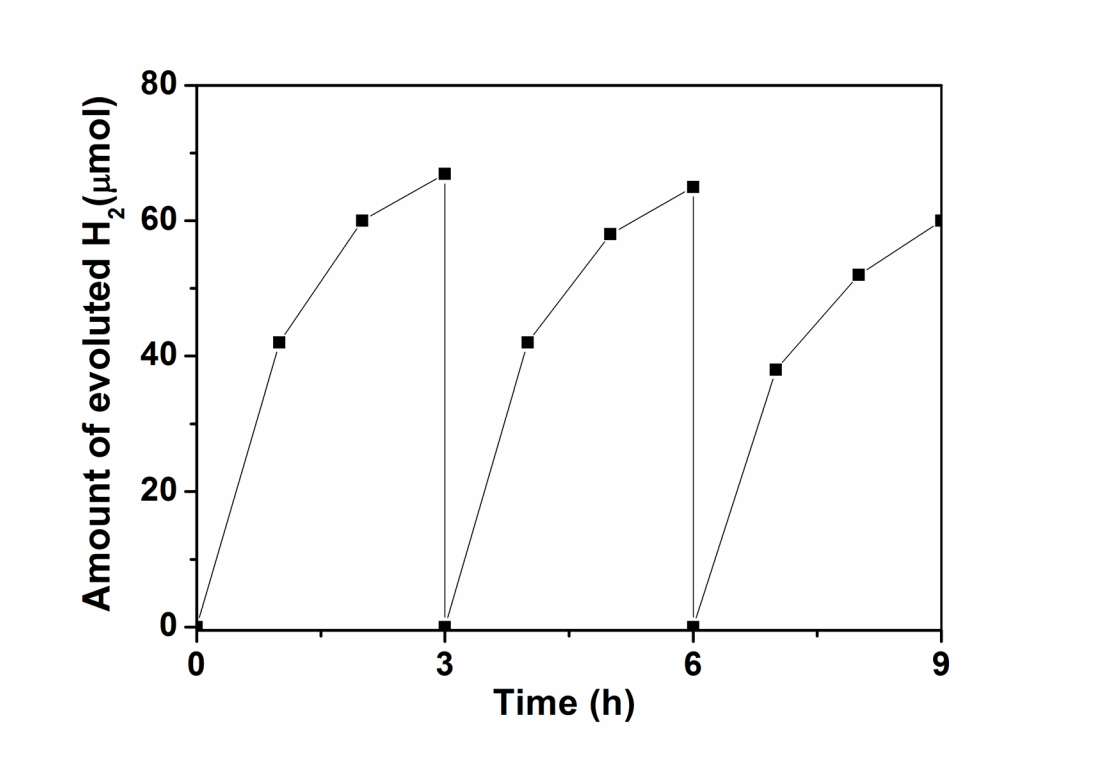

Fig.10. Time course of H_2 evolution from photocatalytic reaction with complex $[Cu_6I_6(ppda)_2]$.

4. Conclusion

This is the first report on efficient white light and the nearest to saturated white emission from the single-molecule hexanuclear Cu(I) iodide nanoclusters with the highest PLQY. Emission color can be largely tuned from blue to white to yellow, by changing the solid state from crystal to powder to film, due to the large structural relaxation, rending a bathochromic shift to the emission. Small S_1–T_1 energy gaps in the solid state indicate that the emission occurs from a thermally activated excited singlet state at ambient temperature. The emission of $[Cu_6I_6(ppda)_2]$ originates from a combination of MLCT and XLCT transitions. Good solubility in organic solvents allows it firstly applied in solution-processed device for hexanuclear Cu iodide nanoclusters. In addition, it shows photocatalytic H_2 evolution activity under visible-light irradiation. This work manifests the great potential of cheap and abundant

neutral Cu(I) halide nanoclusters for emitters in OLEDs and patent light photosensitizer and photocatalyst in H_2 evolution. Obviously, the EQE of device leaves a huge space for further improving the EL performance of copper iodide clusters. Better solubility of the Cu(I) halide nanoclusters in nonpolar solvents is needed to match the requirement for the common host materials.

Conflicts of interest

There are no conflicts to declare.

Acknowledgements

This work was supported by the National Natural Science Foundation of China [grant number 21671061] and application foundation frontier special project by Wuhan Science and Technology Bureau [grant number 2019010701011414]. W.-Y.W. thanks the Hong Kong Research Grants Council (C4006-17G), the Hong Kong Polytechnic University (1-ZE1C) and Ms Clarea Au for the Endowed Professorship in Energy (847S) for the financial support. We thank senior engineer Mingxing Chen (Peking University) for his measurement of photoluminescence property of complex.

Reference

[1] N. Armaroli, G. Accorsi, F. Cardinali, and A. Listorti, In *Photochemistry and Photophysics of Coordination Compounds I*; Eds. V. Balzani, S. Campagna, Springer: Berlin Heidelberg, 2007, **280**, pp 69−115.

[2] Y. Tao, K. Yuan, T. Chen, P. Xu, H. Li, R. Chen, C. Zheng, L. Zhang, and W. Huang, *Adv. Mater*., 2014, **26**, 7931.

[3] M. Hashimoto, S. Igawa, M. Yashima, I. Kawata, M. Hoshino, and M. Osawa, *J. Am. Chem. Soc.*, 2011, **133**, 10348.
[4] R. Hamze,J.L. Peltier, D. Sylvinson, M. Jung, . Cardenas, R. Haiges, M. Soleihavoup, R. Jazzar, P. I. Djurovic, G. Bertrand and M. E. Thompson. *Science*, 2019, **363**, 601-606.
[5] D. Volz, Y. Chen, M. Wallesch, R. Liu,C. Fléchon, D. M. Zink, J. Friedrichs, H. Flügge , R. Steininger, J. Göttlicher, C. Heske, L. Weinhardt, S. Bräse, F. So, and T. Baumann, *Adv. Mater.*, 2015, **27**, 2538.
[6] J. Zhang, C. Duan, C. Han, H. Yang, Y. Wei, and H. Xu, *Adv. Mater.*, 2016, **28**, 5975.
[7] Q. Zhang, Q. Zhou, Y. Cheng, L. Wang, D. Ma, X. Jing, and F. Wang, *Adv. Mater.*, 2004, **16**, 432.
[8] N. Armaroli, G. Accorsi, M. Holler, O. Moudam, J. F. Nierengarten, Z. Zhou, R. T. Wegh, and R. Welter, *Adv. Mater.*, 2006, **18**, 1313.
[9] D. G. Cuttell, S. M. Kuang, P. E. Fanwick, D. R. McMillin, and R. A. Walton, *J. Am. Chem. Soc.*, 2002, **124**, 6.
[10] Z. Liu, M. F. Qayyum, C. Wu, M. T. Whited, P. I. Djurovich, K. O. Hodgson, B. Hedman, E. I. Solomon, and M. E. Thompson, *J. Am. Chem. Soc.*, 2011, **133**, 3700.
[11] D. Asil, J. A. Foster, A. Patra, X. de Hatten, J. del Barrio, O. A. Scherman, J. R. Nitschke, and R. H. Friend, *Angew. Chem. Int. Ed.*, 2014, **53**, 8388.
[12] X. de Hatten, D. Asil, R. H. Friend, and J. R. Nitschke, *J. Am. Chem. Soc.*, 2012, **134**, 19170.
[13] W. Liu, Y. Fang, G. Z. Wei, S. J. Teat, K. Xiong, Z. Hu, W. P. Lustig, and J. Li, *J. Am. Chem. Soc.*, 2015, **137**, 9400.
[14] T. Hasegawa, A. Kobayashi, H. Ohara, M. Yoshida, and M. Kato, *Inorg. Chem.,* 2017, **56**, 4928.
[15] C. W. Hsu, C. C. Lin, M. W. Chung, Y. Chi, G. H. Lee, P. T. Chou, C. H. Chang, and P. Y. Chen, *J. Am. Chem. Soc.*, 2011, **133**, 12085.
[16] X. C. Shan, F. I. Jiang, D. Q. Yuan, H. B. Zhang, M. Y. Wu, L. Chen, J. Wei, S. Q. Zhang, J. Pan, and M. C. Hong, *Chem. Sci.*, 2013, **4**, 1484.
[17] Y. Fang, W. Liu, S. J. Teat, G. Dey, Z. Shen, L. An, D. Yu, L. Wang, D. M. O'Carroll, and J. Li, *Adv. Funct. Mater.*, 2017, **27**, 1603444.
[18] L. Ma, W. Chen, G. Schatte, W. Wang, A. G. Joly, Y. Huang, R. Sammynaiken, and M. Hossu, *J. Mater. Chem. C*, 2014, **2**, 4239.
[19] M. Xie, C. Han, J. Zhang, G. Xie, and H. Xu, *Chem. Mater.*, 2017, **29**, 6606.
[20] (a) M. Osawa, M. Hoshino, M. Hashimoto, I. Kawata, S. Igawa, and M. Yashima, *Dalton Trans.*, 2015, **44**, 8369; (b) Q. Wei, R. Zhang, L. Liu, X. Zhong, L. Wang, G. Li, F. Li, K. A. Alamry and Y. Zhao, *Dalton Trans.*, 2019, **48**, 11448; (c) B. K. Guo, F. Yang, Y. Q. Wang, Q. Wei, L. Liu, X. X. Zhong, L. Wang, J. K. Gong, F. B. Li, W. Y. Wong, K. A. Alamry, Y. Zhao, *J. Lumin.* 2020, **220**, 116963.
[21] X. Hong, B. Wang, L. Liu, X. X. Zhong, F. B. Li, L. Wang, W. Y. Wong, H. M. Qin, and Y. H. Lo, *J. Lumin.*, 2016, **180**, 64.
[22] (a) W. J. Zhang, Z. X. Zhou, L. Liu, X. X. Zhong, A. M. Asiri, K. A. Alamry, F. B. Li, N. Y. Zhu, W. Y. Wong, and H. M. Qin, *J. Lumin.*, 2018, **196**, 425; (b) J. Zhang, C. Duan, C. Han, H. Yang, Y. Wei, and H. Xu, *Adv. Mater.*, 2016, **28**, 5975.

[23] A. Tsuboyama, K. Kuge, M. Furugori, S. Okada, M. Hoshino, and K. Ueno, *Inorg. Chem.*, 2007, **46**, 1992.
[24] D. M. Zink, M. Bächle, T. Baumann, M. Nieger, M. Kühn, C. Wang, W. Klopper, U. Monkowius, T. Hofbeck, H. Yersin, and S. Bräse, *Inorg. Chem.*, 2013, **52**, 2292.
[25] M. J. Leitl, F. R. Küchle, H. A. Mayer, L. Wesemann, and H. Yersin, *J. Phys. Chem. A,* 2013, **117**, 11823.
[26] T. Hofbeck, U. Monkowius, and H. Yersin, *J. Am. Chem. Soc.*, 2015, **137**, 399.
[27] I. Bonnaventure, and A. B. Charette, *J. Org. Chem.*, 2008, **73**, 6330.
[28] *SAINT Reference Manual*, Siemens Energy and Automation, Madison, WI, 1994.
[29] G. M. Sheldrick, *SADABS*, *Empirical Absorption Correction Program*, University of Göttingen, Göttingen, Germany, 1997.
[30] G. M. Sheldrick, *SHELXTL Reference Manual*, *Version 5.1*, Siemens Energy and Automation, Madison, WI, 1997.
[31] (a) M. J. Frisch, G. W. Trucks, H. B. Schlegel, G. E. Scuseria, M. A. Robb, J. R. Cheeseman, G. Scalmani, V. Barone, B. Mennucci, G. A. Petersson, H. Nakatsuji, M. Caricato, X. Li, H. P. Hratchian, A. F. Izmaylov, J. Bloino, G. Zheng, J. L. Sonnenberg, M. Hada, M. Ehara, K. Toyota, R. Fukuda, J. Hasegawa, M. Ishida, T. Nakajima, Y. Honda, O. Kitao, H. Nakai, T. Vreven, J. A. Montgomery Jr, J. E. Peralta, F. Ogliaro, M. Bearpark, J. J. Heyd, E. Brothers, K. N. Kudin, V. N. Staroverov, R. Kobayashi, J. Normand, K. Raghavachari, A. Rendell, J. C. Burant, S. S. Iyengar, J. Tomasi, M. Cossi, N. Rega, J. M. Millam, M. Klene, J. E. Knox, J. B. Cross, V. Bakken, C. Adamo, J. Jaramillo, R. Gomperts, R. E. Stratmann, O. Yazyev, A. J. Austin, R. Cammi, C. Pomelli, J. W. Ochterski, R. L. Martin, K. Morokuma, V. G. Zakrzewski, G. A. Voth, P. Salvador, J. J. Dannenberg, S. Dapprich, A. D. Daniels, O. Farkas, J. B. Foresman, J.V . Ortiz, J. Cioslowski, and D. J. Fox, *Gaussian 09*, *Revision A.1*, Gaussian Inc., Wallingford, CT, 2016; (b) G. M. Sheldrick. *Acta Cryst.*, 2008, **112**, A64.
[32] Q. Hou, J. H. Yu, J. N. Xu, Q. F. Yang, and J. Q. Xu, *Cryst. Eng. Comm.*, 2009, **11**, 2452.
[33] C. Kutal, *Coord. Chem. Rev.*, 1990, **99,** 213.
[34] H. Yersin, A. F. Rausch and R. Czerwieniec, in *Physics of Organic Semiconductors*, ed. W. Bruetting, C. Adachi and R. J. Holmes, Wiley-VCH, Weinheim, 2012, p. 371.